Association of Cl with C_2H_2 by unified variable-reaction-coordinate and reaction-path variational transition-state theory

Linyao Zhang[a,b,c], Donald G. Truhlar[b,c,1], and Shaozeng Sun[a,1]

[a]School of Energy Science and Engineering, Harbin Institute of Technology, 150001 Harbin, People's Republic of China; [b]Department of Chemistry, Chemical Theory Center, University of Minnesota, Minneapolis, MN 55455; and [c]Supercomputing Institute, University of Minnesota, Minneapolis, MN 55455

Contributed by Donald G. Truhlar, January 15, 2020 (sent for review November 14, 2019; reviewed by Stephen J. Klippenstein and Paul Marshall)

Barrierless unimolecular association reactions are prominent in atmospheric and combustion mechanisms but are challenging for both experiment and kinetics theory. A key datum for understanding the pressure dependence of association and dissociation reactions is the high-pressure limit, but this is often available experimentally only by extrapolation. Here we calculate the high-pressure limit for the addition of a chlorine atom to acetylene molecule (Cl + C_2H_2→C_2H_2Cl). This reaction has outer and inner transition states in series; the outer transition state is barrierless, and it is necessary to use different theoretical frameworks to treat the two kinds of transition state. Here we study the reaction in the high-pressure limit using multifaceted variable-reaction-coordinate variational transition-state theory (VRC-VTST) at the outer transition state and reaction-path variational transition state theory (RP-VTST) at the inner turning point; then we combine the results with the canonical unified statistical (CUS) theory. The calculations are based on a density functional validated against the W3X-L method, which is based on coupled cluster theory with single, double, and triple excitations and a quasiperturbative treatment of connected quadruple excitations [CCSDT(Q)], and the computed rate constants are in good agreement with some of the experimental results. The chlorovinyl (C_2H_2Cl) adduct has two isomers that are equilibrium structures of a double-well C≡C–H bending potential. Two procedures are used to calculate the vibrational partition function of chlorovinyl; one treats the two isomers separately and the other solves the anharmonic energy levels of the double well. We use these results to calculate the standard-state free energy and equilibrium constant of the reaction.

kinetics | transition state | rate constant | electronic structure | direct dynamics

Radical–molecule reactions are central to many branches of chemistry, and such reactions dominate gas-phase combustion and atmospheric chemistry (1–4). Barrierless reactions are a special case of particular interest and provide great challenges for reaction kinetics theory (5–9). In the absence of a potential energy barrier, one must find the transition state by a free-energy criterion (10, 11), i.e., by variational transition-state theory (VTST) (12–14). The most widely applied form of VTST (12, 13), sometimes called reaction-path VTST (RP-VTST), is based on passage of reactive flux through a tight TS, by which we mean that the flux through the variationally best TS is in a region differing from a minimum energy path only by small-amplitude vibrations and possibly one or more one-dimensional internal rotations. However, this is not generally adequate at loose TSs such as encountered in barrierless association reactions (15–17). The state of the art for treating the loose TSs is variable-reaction-coordinate VTST (VRC-VTST) with a multifaceted dividing surface, as developed by Georgievskii and Klippenstein (18–20). Another complication is that such barrierless associations often have a tight inner TS as well as a loose outer one; the two TSs may need to be treated by the two different forms of VTST. The rate constant should be calculated taking account of both TSs (11, 21–27).

In the present article we study the addition reaction

$$Cl + C_2H_2 \rightarrow \beta\text{-}C_2H_2Cl, \qquad [1]$$

where we carry out calculations for the condition where the pressure is high enough that the kinetics is in the pressure-independent second-order regime. The temperature and pressure dependence of reaction **1** have been studied both experimentally (28–36) and theoretically (36, 37). Experimental measurements of association rate constants generally do not go to high enough pressure to measure the high-pressure equilibrium limit directly, and this limit is obtained by theory-guided extrapolation. The kind of difficulty one faces in analyzing experimental data on association and dissociation reactions is well illustrated by the comments of Knyazev et al. (38) on the reaction system Cl + C_2H_4 ⇌ C_2H_4Cl, which is similar to reaction **1** studied here. Discussing their extraction of high-pressure-limit rate constants from the raw experimental data, they said, "One should bear in mind that the above model of the reaction is based on significant simplifications. . .. Different temperature dependencies of the collisional parameters and a different (within uncertainties) heat of formation of CH_2CH_2Cl will result in different values of rate constants. Moreover, the simplifications of the model (e.g., the assumption of a fixed TS and the representation of the tumbling motion of the C_2H_4 fragment relative to the Cl atom in the TS with low-frequency vibrational modes) result in uncertainties which are not easily estimated." The present treatment of Cl + C_2H_2 → C_2H_2Cl attempts to overcome these sources of uncertainty by directly calculating the

Significance

A key issue in chemical kinetics is advancing the theoretical framework to handle reactions beyond the domain of textbook transition-state theory by including—for example—anharmonicity, barrierless transition states, transition states in series, and the effect of conformational flexibility on equilibrium constants. Other key issues are validating affordable electronic structure methods for direct dynamics and the direct calculation of high-pressure limiting rate constants, which are often obtainable experimentally only by extrapolation. The present article addresses all these issues for a prototype radical–molecule association reaction and thereby demonstrates how to combine improved theoretical methods to provide rate constants in cases where experimental data are uncertain or missing.

Author contributions: L.Z., D.G.T., and S.S. designed research; L.Z. and D.G.T. performed research; L.Z. and D.G.T. analyzed data; and L.Z. and D.G.T. wrote the paper.

Reviewers: S.J.K., Argonne National Laboratory; and P.M., University of North Texas.

The authors declare no competing interest.

Published under the PNAS license.

[1]To whom correspondence may be addressed. Email: truhlar@umn.edu or sunsz@hit.edu.cn.

This article contains supporting information online at https://www.pnas.org/lookup/suppl/doi:10.1073/pnas.1920018117/-/DCSupplemental.

Downloaded by guest on October 22, 2020

high-pressure limit rather than extrapolating to it, by using high-level electronic structure data to pin down the energetics, and by using VRC-VTST to eliminate the oversimplified treatment of the low-frequency vibrational modes.

We use the canonical unified statistical (CUS) (14, 27) theory to combine a VRC-VTST treatment of the outer TS with an RP-VTST treatment of the inner one to study the reaction in high-pressure limit. The microcanonical and E,J-resolved unified statistical models are also feasible, and might be more appropriate at pressures where the intermediate complex does not suffer enough collisions with the bath gas for thermalization (39–41).

The product, β-chlorovinyl, has the radical site on the α-carbon and the chlorine on the β-carbon (Fig. 1). This reaction is barrierless (36, 42) and serves as a prototype for barrierless addition of a doublet radical to a π-bond of an alkene or alkyne. Some previous closely related applications of VTST are studies of the addition reaction of OH to ethylene (39), the abstraction reaction of CN with ethane (40), the reactions of oxygen atoms with alkenes (41), and the addition of singlet methylene to acetylene (43). The only previous example we know of where VRC-VTST, RP-VTST, and CUS theory were applied together is the work of Monge-Palacios et al. (44) on HO_2 + propen-2-ol.

Methods and Theoretical Considerations. Electronic structure energies including nuclear repulsion but with neither zero-point energy nor vibrational-rotational thermal energies are potential energies for nuclear motion. The (classical) barrier heights and reaction energies are computed from potential energies. Adding zero-point energy gives the enthalpies of activation and enthalpies of reaction at 0 K. Finite-temperature enthalpies of activation, enthalpies of reaction, free energies of activation, and free energies of reaction are obtained by adding thermal contributions.

Validation of a Density Functional. The present calculations are carried out by direct dynamics (45, 46). In direct dynamics, one calculates the energy, gradient, and Hessian directly each time they are needed by the dynamics algorithm (rather than fitting the potential energy surface). Because direct dynamics is too expensive for the highest possible levels of electronic structure theory, our first step is to compare affordable Kohn–Sham density-functional theory to benchmark calculations at stationary points (saddle points and equilibrium structures) to select and validate a density-functional method (DFM) that is accurate for this particular reaction and that can be used for direct dynamics. A DFM is a combination of an approximate exchange-correlational functional and basis set. We tested two density functionals, M06-2X (47) and M08-HX (48), that were previously shown to perform quite well for main-group thermochemistry and kinetics. They were combined with three polarized triple-ζ basis sets, jun-cc-pVTZ (49, 50), may-cc-pVTZ (49, 50), and MG3S (51).

The W3X-L method (52), which is a post-CCSD(T) method, where CCSD(T) denotes coupled cluster theory with single and double excitations and a quasiperturbative treatment of connected triple excitations was used to obtain a benchmark energy for each optimized geometry. The W3X-L protocol employs carefully selected basis sets to accurately approximate CCSDT(Q)/CBS results (coupled-cluster theory with single, double, and triple excitations and a quasiperturbative treatment of connected quadruple excitations with a complete basis set).

For each DFM, we optimized the geometries of all 14 stationary points (see *SI Appendix* for figures and tables specifying these points), and we ran single-point W3X-L calculations at those geometries. Comparing with benchmark results (detailed results for this step are in *SI Appendix*), we found that M06-2X/may-cc-pVTZ has the lowest mean unsigned error (MUE), and therefore we selected this DFM for direct dynamics calculations. The MUE is 0.66 kcal/mol, which is within the widely used criterion of 1 kcal/mol for "chemical accuracy."

Validation of WMS. We also compared the W3X-L results to the more recent Wuhan–Minnesota scaling (WMS) (53) composite model chemistry method, and this comparison shows that the two methods agree quite well, with WMS being much less expensive.

Kinetics. All rate constant calculations correspond to equilibrated reactants and intermediates, and all chlorovinyl radicals produced are assumed to be stabilized. This assumption is valid at high enough pressures. The lower-pressure situation is not treated in the present study.

Reaction-path VTST. For the inner TS, we calculated the isoinertial-coordinate minimum energy path (54) (MEP) through the saddle point. This MEP is treated as the reaction path, and we performed vibrational analysis transverse to this path by using curvilinear coordinates (55); *SI Appendix*, Fig. S1. Then we searched along the reaction path to obtain the variationally best dividing surface, which is the variational TS (VTS). This produces the canonical RP-VTST rate constant, which can be written as

$$k_{\text{inner}} = \kappa \frac{k_B T}{h} \frac{\Phi^{\text{VTS}}}{\Phi^{\text{R1}}\Phi^{\text{R2}}} \exp\left(-\frac{V_{\text{MEP}}^{\text{VTS}}}{k_B T}\right), \qquad [2]$$

where κ is the tunneling transmission coefficient, k_B is the Boltzmann constant, h is Planck's constant, Φ is a partition function per unit volume (with the zero of energy at the local potential energy minimum) for the VTS or one of the reactants (R1 and R2), and $V_{\text{MEP}}^{\text{VTS}}$ is the potential energy of the VTS relative to reactants.

Eq. **2** can be rewritten in terms of the standard-state free energy of activation at the VTS $\Delta G_T^{\text{VTS,inner,o}}$ as

$$k_{\text{inner}} = \kappa \frac{k_{\text{B}} T}{h} \left(\frac{k_{\text{B}} T}{P^{\text{o}}}\right) \exp\left(-\frac{\Delta G_T^{\text{VTS,inner,o}}}{k_B T}\right), \qquad [3]$$

where P^{o} is the standard pressure (1 bar).

We replaced the DFM potential energies with the W3X-L benchmark ones in the calculation of k_{inner} to get more accurate results; we corrected the barrier for all variational dividing surfaces by using the correction obtained at the saddle point.

VRC-VTST. For loose transition states, it is difficult to define a useful reaction path because some of the internal coordinates have multidimensional wide-amplitude motion. We therefore use VRC-VTST with multifaceted dividing surfaces, as proposed by Georgievskii and Klippenstein (18–20), and in particular, we use the implementation (56) in the *Polyrate* (57) computer program. The reaction coordinate for the VRC scheme is defined by pivot

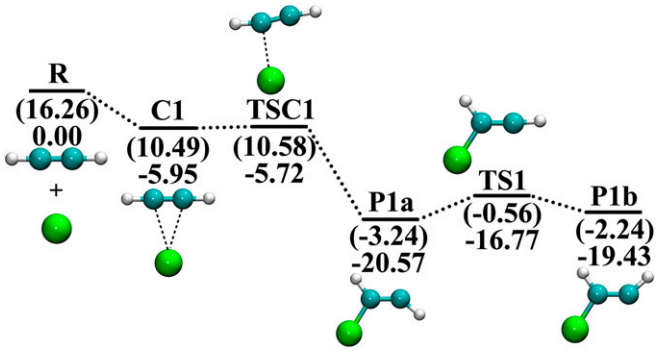

Fig. 1. M06-2X/may-cc-pVTZ stationary points (in kcal/mol) on the PES along the main association path for the Cl + C_2H_2 reaction with energies relative to the sum of the energies of the separated reactants. The values in parentheses include zero-point energies, i.e., they are relative enthalpies at 0 K.

Downloaded by guest on October 22, 2020

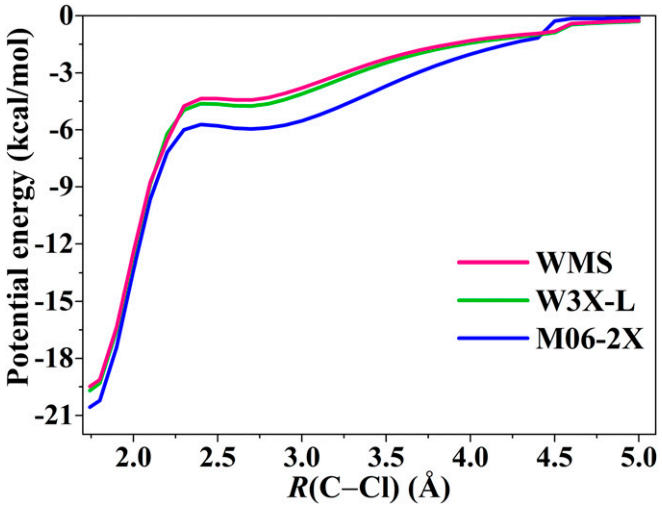

Fig. 2. Relaxed scan of electronic potential energies (in kcal/mol) along the C(1)–Cl distance (Å) calculated by M06-2X/may-cc-pVTZ and two high-level composite model chemistry methods (W3X-L and WMS); the zeros of the energies are set as the sum of the energies of separated reactants.

points as explained previously (14, 20, 58). We place one pivot point ($j = 1$) on the Cl atom and one on each C atom ($j = 2, 3$); see *SI Appendix*, Fig. S2. The reaction coordinate s is the minimal value of r_{12} and r_{13}, where r_{1j} is the distance between pivot points 1 and j. In this way the dividing surface has two facets. It would be interesting to study the dependence of the results on optimizing the pivot points or using a fixed center-mass separation instead of putting the pivot points on the reactive atoms.

For reactions with loose TSs, VRC-VTST divides the motions into conserved modes and transitional modes. The conserved modes are the vibrational modes of the separated fragments (reactants), and we assume the contribution of the conserved modes to the TS partition function cancels with the contribution of these modes to the reactant partition function. The transitional modes of the TS include the fragment rotations and the radial and orbital components of the relative translation; these are converted to vibrational modes and overall rotation of the adduct species. The contribution of transitional modes to TS partition function is evaluated via Monte Carlo integration of classical phase space. The rate constant by energy- and total-angular-momentum-resolved microcanonical VRC-VTST (which we will abbreviate in this article as *E,J*-μVT) for an association reaction is then given as

$$k_{\text{outer}} = g_e \frac{Q_{\text{trans}}^{\text{E,J-}\mu\text{VTS}}}{hQ_{\text{rot}}^{\text{R1}}Q_{\text{rot}}^{\text{R2}}\Phi_{\text{rel}}}, \qquad [4]$$

where g_e is the ratio of the electronic partition function of the TS to that of the reactants; $Q_{\text{rot}}^{\text{R1}}$ and $Q_{\text{rot}}^{\text{R2}}$ are the rotational partition functions of the reactants; Φ_{rel} is the relative translational partition function per unit volume of the separated reactants; and $Q_{\text{trans}}^{\text{E,J-}\mu\text{VTS}}$ is the partition function for the translational modes, as given by

$$Q_{\text{trans}}^{\text{E,J-}\mu\text{VTS}} = \left(\frac{1}{\sigma^{\ddagger}}\right) \iint_{E,J} N_{\text{trans}}^{\text{E,J-}\mu\text{VTS}}(E,J) e^{-E/k_B T} \mathrm{d}E\mathrm{d}J, \qquad [5]$$

where $\sigma^{\ddagger}$ is the rotational symmetry number of the TS (see further discussion in *SI Appendix* for its definition); and $N_{\text{trans}}^{\text{E,J-}\mu\text{VTS}}(E,J)$ is the number of vibrational-rotational accessible states of the generalized TS calculated with the optimum s for each energy E and total angular momentum J. Details of the calculation of $N_{\text{trans}}^{\text{E,J-}\mu\text{VTS}}(E,J)$ and the integral have been given previously (14, 58).

Canonical unified statistical theory. The canonical unified statistical (14, 27) (CUS) theory provides a way to include the effect of two TSs in series. [For TSs in parallel, one would use MS-VTST or MP-VTST (14, 59).] The CUS rate constant k_{CUS} can be expressed in terms of k_{outer} (the rate constant for passing through the outer TS), k_{inner} (the rate constant for passing through the inner TS), and k_{complex} (the rate constant for maximum flux through the intermediate between the two TSs) as follows (14):

$$\frac{1}{k_{\text{CUS}}} = \begin{cases} \dfrac{1}{k_{\text{outer}}} + \dfrac{1}{k_{\text{inner}}} - \dfrac{1}{k_{\text{complex}}}, & \Delta G_T^{\text{VTS,inner,o}} > 0 \\ \dfrac{1}{k_{\text{outer}}}, & \text{otherwise} \end{cases}. \qquad [6]$$

We obtained k_{outer} and k_{inner} by VRC-VTST and RP-VTST, respectively, and k_{complex} is approximated using Eq. **3** by assuming the local stable complex between the two TSs is a generalized TS and therefore omitting its 85-cm^{-1} vibration that has a normal mode character similar to the imaginary vibration of the inner saddle point (*SI Appendix*, Fig. S3). We have also replaced the DFM potential energies with the W3X-L benchmark ones in the calculation of k_{complex}.

Equilibrium Constants. We also calculate the K_c so that the reverse rate constant k_{-1} can be obtained from the forward rate constant k_{CUS} by detailed balance as

$$k_{-1} = k_{\text{CUS}}/K_c. \qquad [7]$$

The equilibrium constant for the association reaction was computed by

$$K_c(T) = \left(\frac{k_B T}{P^0}\right) \exp\left(-\frac{\Delta G_T^{\circ}}{k_B T}\right), \qquad [8]$$

where ΔG_T° is the standard-state free energy of reaction at temperature T. In this calculation, the DFM potential energies

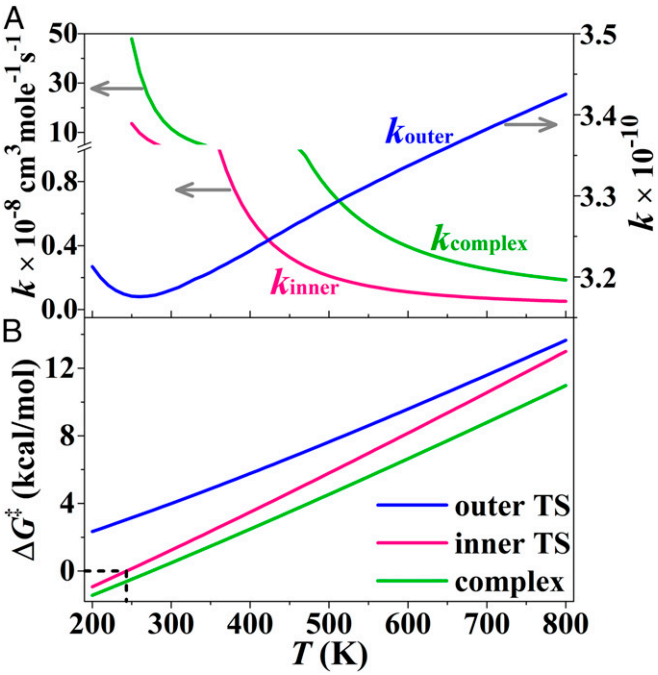

Fig. 3. (*A*) Rate constants k_{outer} and k_{inner}, reactive flux coefficients k_{complex}, and (*B*) free energies of activation for the outer TS, the inner TS, and the complex. The values for the outer TS are obtained from k_{outer}, and the potential energies for the inner TS and the complex are corrected with W3X-L benchmark results.

Downloaded by guest on October 22, 2020

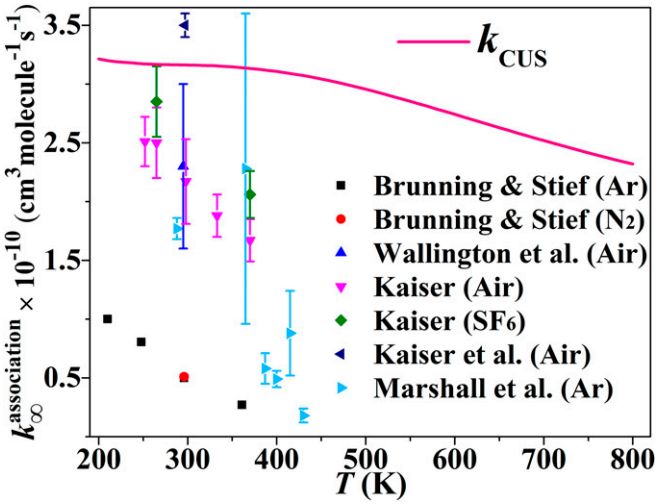

Fig. 4. The calculated and experimental high-pressure limit association rate constants for the reaction Cl + C_2H_2 → C_2H_2Cl. The bath gas used in each experiment is given in parentheses.

are replaced with the W3X-L benchmark results for better accuracy.

One complication in calculating ΔG_T° is the existence of two conformations of the product β-chlorovinyl, as shown in Fig. 1, in particular *trans* β-chlorovinyl (P1a) and *cis* β-chlorovinyl (P1b). The isomerization between two conformations via C≡C–H bending has a modest barrier (3.94 kcal/mol by W3X-L, 3.90 by WMS, 3.80 by M06-2X/may-cc-pVTZ; 2.68 kcal/mol if we add zero-point energy to get an enthalpy of activation at 0 K) so we treat the two conformations as being in equilibrium. Two procedures were used to treat the conformations for the calculation of equilibrium constants.

The first procedure is to treat the conformations independently. The total equilibrium constant for reaction **1** is then the sum (60, 61):

$$K_c = K_{c,trans} + K_{c,cis}. \quad [9]$$

The second procedure recognizes that the C≡C–H bending mode of β-chlorovinyl is a double-well potential and treats the two conformations as a single isomer with a double-well vibration. The partition function for this mode is obtained by solving for the anharmonic energy levels of the double-well potential by using the WKB method.

Data Availability Statement. All data discussed in the paper are available in the main text or *SI Appendix*.

Results and Discussion

Potential Energy Surface. The potential energy surface (PES) for reaction **1** is shown in Fig. 1. A more complete diagram including some higher-energy species is given in *SI Appendix*, Fig. S4. The stationary points are consistent with previous theoretically studies (36, 37). To validate the DFM, we first optimized each stationary geometry using a given DFM; then we did single-point calculation with W3X-L for each DFM-optimized geometry. In *SI Appendix*, Tables S1 and S2, we give the comparisons for the M06-2X and M08-HX functionals with three triple-ζ basis sets. The comparison shows that M06-2X/may-cc-pVTZ DFM gives the smallest MUE (0.66 kcal/mol) for the relative energies of the stationary points and also gives a small mean signed error (–0.47 kcal/mol).

We have previously shown that M06-2X and M08-HX yield reasonably accurate geometries for TSs (62). *SI Appendix*, Tables S1 and S2 show that the high-level calculations give almost the same energy for structures optimized with different DFMs; this adds confidence that any errors in the density-functional geometries do not cause a large error in the present results.

To further validate the DFM, we performed a relaxed scan along the association path of the reaction Cl + C_2H_2 [doing constrained optimization at each fixed C(1)–Cl distance] with M06-2X/may-cc-pVTZ. Benchmark energies were calculated by W3X-L and WMS for each geometry along the relax scan curve. The DFM curve and the benchmark curves are shown in Fig. 2 with the zero of energies at the separated reactants. The energy deviations of the selected DFM compared with W3X-L are less than 1.5 kcal/mol in the whole range of 2.5–5.0 Å, and the deviations in the important VST region (see the contour map given in *SI Appendix*, Fig. S5) of 4.0–4.5 Å (where the loose outer TS is located) are even smaller (less than 0.6 kcal/mol). On the bases of the tests described in this paragraph and the previous two paragraphs and of the affordable cost of M06-2X/may-cc-pVTZ, we decided that M06-2X/may-cc-pVTZ provides a good compromise between accuracy and computational cost for our direct dynamics calculations.

The difference between the two high-level composite methods is less than 0.4 kcal/mol for the geometries of the relaxed scan, which lends further support to the accuracy of both benchmark calculations and—which can be very important for future work—shows that the WMS methods can give quite accurate results at a relatively low computational cost. The average ratio of the computer time for WMS as compared to W3X-L is 0.076, which is averaged over 34 calculations of the relaxed scan (Fig. 2).

In *SI Appendix*, Table S3, we list the unscaled harmonic vibrational frequencies of the stationary points using M06-2X/may-cc-pVTZ. In the calculations, these were scaled to obtain more accurate zero-point energies.

Table 1. Calculated (k_{CUS}) and experimental high-pressure limit association rate constants $k_\infty^{association}$ (in the units of 10^{-10} cm^3 $molecule^{-1}\cdot s^{-1}$) at various temperatures

Ref.	Authors, year	T, K	Experiment	k_{CUS}	k_{CUS}/Exp.
30	Brunning and Stief (1985)	210	1.00*	3.20	3.2
		248	0.80*	3.17	4.0
		296	0.50*	3.16	6.3
		361	0.27*	3.14	12
32	Wallington et al. (1990)	295	2.3 ± 0.7†	3.16	1.4
33	Kaiser (1992)	252	2.5 ± 0.2†	3.17	1.3
		265	2.6 ± 0.5‡	3.17	1.2
		298	2.2 ± 0.4†	3.16	1.4
		333	1.9 ± 0.2†	3.15	1.7
		370	1.9 ± 0.4‡	3.13	1.6
34	Kaiser and Wallington (1996)	297	3.5§	3.16	0.9
63	NASA (2003)	250	2.5 ± 0.4¶	3.17	1.3
		298	2.1 ± 0.4¶	3.16	1.5
		370	1.7 ± 0.4¶	3.13	1.8
36	Gao et al. (2007)	288	1.77 ± 0.18†	3.16	1.8
		365	2.28 ± 2.64†	3.14	1.4
		387	0.58 ± 0.26†	3.12	5.4
		400	0.49 ± 0.14†	3.11	6.3
		415	0.88 ± 0.36†	3.09	3.5
		430	0.18 ± 0.06†	3.07	17
64	NASA (2015)	250	2.5 ± 0.4¶	3.17	1.3
		298	2.2 ± 0.4¶	3.16	1.4
		370	1.9 ± 0.4¶	3.13	1.6

*High-pressure limit.
†High-pressure limit with 2σ error bars.
‡Range includes high-pressure limits obtained with two different bath gases.
§High-pressure limit obtained with best fit to data. Another fit gave 2.0.
¶NASA recommendation.

Downloaded by guest on October 22, 2020

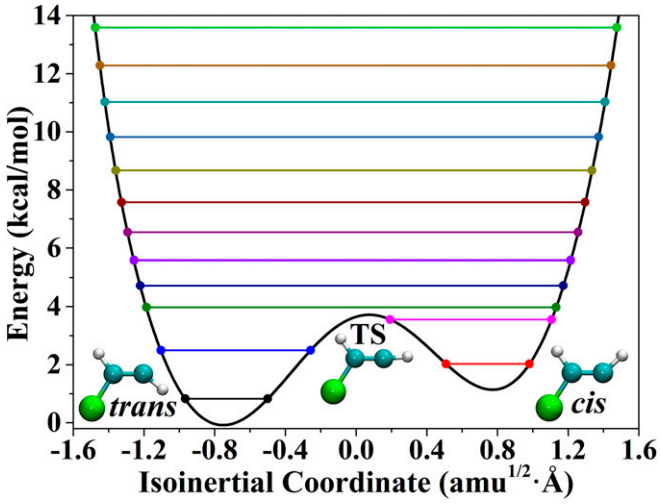

Fig. 5. The double-well potential for the C≡C–H bending in β-chlorovinyl calculated by M06-2X/may-cc-pVTZ and the associated anharmonic vibrational energy levels obtained by WKB method. Zero of the *x* axis is linear C≡C–H with negative and positive coordinates correspond to *trans* and *cis* conformation, respectively.

Association Rate Constants. The rate constants k_{outer}, k_{inner}, and $k_{complex}$ (the data are given in *SI Appendix*, Table S4) are plotted in Fig. 3*A*, and the corresponding free energies of activation for the three rate constants are given in Fig. 3*B*. (Tabular presentations of rate constants are available in *SI Appendix*, Tables S4 and S5.) The temperature dependence for k_{outer} is negative for $T < \sim 260$ K and positive at higher T, while the T dependences of k_{inner} and $k_{complex}$ are negative at all T. In *SI Appendix*, Table S4, we show that for $T < 450$ K, the outer TS yields a rate smaller than the inner one by a factor of 10 (450 K) to 3,700 (200 K); however the inner TS reduces the rate constant by 19, 18, 25, and 32% at 500, 600, 700, and 800 K, respectively.

The experimental measurements do not go to high enough pressure to directly measure the high-pressure limit, but three groups have attempted to extract the high-pressure limit by fitting the pressure dependence with theoretical guidance. The inferred high-pressure rate constants are given in Table 1 (30, 32–34), and some of them are plotted in Fig. 4; the table and figure include comparisons to our CUS rate constants. Table 1 also includes the 2003 and 2015 NASA recommendations (63, 64), which are based on the measurements of Kaiser (33) and Kaiser and Wallington (34). All of the experimental evaluations indicate the high-pressure limit rate constant has a negative temperature dependence in the available experimental temperature range of 210 to 430 K, and this is also found in the present calculations. Brunning and Stief (30) and Gao et al. (36) predicted a significant decrease in the higher-temperature part of the range, but a much smaller decrease is seen in the work of Kaiser (33) or the present calculations. Our calculated k_{CUS} rate constants show only an ~3% decrease over the experimental temperature range.

We fit the calculated rate constants to our previously (59, 65) recommended four-parameter function, which gives

$$k_{CUS} = 2.966\times10^{-9}\text{cm}^3\text{molecule}^{-1}\cdot\text{s}^{-1}\left(\frac{T+225.34}{300}\right)^{-1.654}\exp\left(-\frac{0.698(T+225.34)}{R(T^2+225.34^2)}\right), \quad [10]$$

where $R = 1.9872\times10^{-3}$ kcal mol^{-1}·K^{-1}.

Association Equilibrium Constant. The bending potential that connects the two β-chlorovinyl conformations is a double-well potential. This anharmonic property increases the C_2H_2Cl density of states (37) and therefore increases the association equilibrium constants. To study the influence of this anharmonic vibration, we used the WKB approximation to solve the one-dimensional Schrödinger equation in isoinertial (54, 66) coordinates for the vibrational energy levels of the C≡C–H bending mode; the *trans* β-chlorovinyl was used, and the double-well bending potential calculated by a relaxed scan with M06-2X/may-cc-pVTZ and fitted to eighth-order polynomial, as shown in Fig. 5, which also shows the first few energy levels (the energy levels and inner and outer turning points for each level are listed in *SI Appendix*, Table S6). The distance in isoinertial coordinates between two geometries along the relaxed scan is obtained by orienting the points along the path using Chen's method (67).

There are three vibrations (350, 694, and 821 cm^{-1}, *SI Appendix*, Fig. S6) of the *trans* β-chlorovinyl that show C≡C–H bending character. (All vibrational frequencies mentioned in this paragraph are the unscaled ones.) The normal modes and harmonic frequencies (*SI Appendix*, Figs. S6–S8) of these vibrations indicate that the 694-cm^{-1} vibration is the one corresponding to the C≡C–H double-well potential. This compares well to the harmonic frequency of 677 cm^{-1} on our fitted bend. We may compare this aspect of our calculations to the work of Gao et al. (36), who also computed the anharmonic vibrational levels of the C≡C–H bending for thermochemistry calculations; the C≡C–H bending frequency of the *trans* β-chlorovinyl in their study was 364 cm^{-1} as compared to 694 cm^{-1} here. Consequently we obtained quite different energy levels than Gao et al.

To compute partition functions and free energies of the product, we calculated the partition function for the 694-cm^{-1} mode by summing Boltzmann factors of the WKB energy levels, and we treated the other vibrations (scaled by 0.971 as discussed in *SI Appendix*) by the quasiharmonic oscillator approximation.

The computed equilibrium constants at various temperatures by the above-mentioned two procedures are listed in Table 2 (see *SI Appendix*, Table S7, for results at more temperatures) and compared with available experimental results from Gao et al. (36), The results with the anharmonic bend are larger, which means the anharmonic treatment for the C≡C–H bending has indeed increased the density of states. Although we have corrected the DFM potential energies with W3X-L benchmark values and included the anharmonicity of the C≡C–H anharmonic vibration, our computed values are higher than the experimental results by factors of 8–34. Further experimental and theoretical studies would be desirable to resolve the discrepancy, as there are no other available results for comparing.

Summary

The barrierless addition of Cl atoms to the C_2H_2 molecule has two VTSs in series along the reaction path. We treated one by

Table 2. Calculated and experimental association equilibrium constants K_c (in the units of cm^3 molecule^{-1})

T, K	$K_{exp.}$*	$K_{c,1}$†	$K_{c,1}/K_{exp.}$	$K_{c,2}$‡	$K_{c,2}/K_{exp.}$
365	1.59×10^{-14}	3.33×10^{-13}	20.94	4.17×10^{-13}	26.24
387	6.17×10^{-15}	7.62×10^{-14}	12.35	9.51×10^{-14}	15.41
400	4.41×10^{-15}	3.44×10^{-14}	7.81	4.29×10^{-14}	9.72
415	2.69×10^{-15}	1.46×10^{-14}	5.44	1.82×10^{-14}	6.76
430	1.34×10^{-15}	6.62×10^{-15}	4.94	8.20×10^{-15}	6.12

*Experimental values from ref. 36.
†Calculated by assuming the two β-chlorovinyl conformations are independent.
‡Calculated using the WKB anharmonic energy levels for the C≡C–H bending mode.

Downloaded by guest on October 22, 2020

VRC-VTST and the other by RP-VTST. The CUS model is used to account for the statistical branching probability for the complex to redissociate to reactants. The CUS rate constants successfully agree with the negative temperature dependence of the experimental high-pressure limit association rate constants and are in reasonable agreement with some of the experimental results; they cannot agree with all of the experiments since the experiments differ among themselves, but all of the experimental results indicate a steeper temperature dependence than theory. The association equilibrium constants have also been predicted based on the calculated free energy of reaction, including a treatment of the anharmonicity of the double-minimum C≡C–H bending mode. This anharmonic treatment increases the calculated equilibrium constant, which is larger than the experimental ones. Possible reasons for the remaining differences of experimental and theoretical rate constants include the simplified treatment of reactant and product anharmonicity, the not easily estimated uncertainties in the experiments, and the sensitivity of the results to the details of the electronic structure calculations.

ACKNOWLEDGMENTS. This work was supported in part by the US Department of Energy, Office of Basic Energy Sciences, under Grant DE-SC0015997, and by the National Natural Science Foundation of China under Grant 51536002. L.Z. was supported by a scholarship from the China Scholarship Council (201706120185).

1. W. A. Sanders, M. C. Lin, *Chemical Kinetics of Small Organic Radical*, Z. Alfassi, Ed. (CRC Press, Boca Raton, FL, 1988), vol. III.
2. K. Liu, A. Wagner, Eds., *The Chemical Dynamics and Kinetics of Small Radicals, Part 1* (World Scientific, Singapore, 1995).
3. J. Zádor, C. A. Taatjes, R. X. Fernandes, Kinetics of elementary reactions in low-temperature autoignition chemistry. *Prog. Energ. Combust.* **37**, 371–421 (2011).
4. L. Vereecken, J. S. Francisco, Theoretical studies of atmospheric reaction mechanisms in the troposphere. *Chem. Soc. Rev.* **41**, 6259–6293 (2012).
5. S. J. Klippenstein *et al*., A theoretical and experimental study of the CN + NO association reaction. *J. Phys. Chem. A* **102**, 6973–6980 (1998).
6. L. B. Harding, S. J. Klippenstein, A theoretical analysis of the reaction of H with C_2H_5. *Symp. (Int.). Combust.* **27**, 151–157 (1998).
7. M. A. Blitz, K. J. Hughes, M. J. Pilling, Determination of the high-pressure limiting rate coefficient and the enthalpy of reaction for OH + SO_2. *J. Phys. Chem. A* **107**, 1971–1978 (2003).
8. S. C. Smith, "Recent developments in statistical rate theory for unimolecular and complex-forming reactions" in *Modern Trends in Chemical Reaction Dynamics: Experiment and Theory (Part 1)*, X. Yang, K. Liu, Eds. (World Scientific, Singapore, 2004), pp. 291–327.
9. L. B. Harding, Y. Georgievskii, S. J. Klippenstein, Predictive theory for hydrogen atom-hydrocarbon radical association kinetics. *J. Phys. Chem. A* **109**, 4646–4656 (2005).
10. B. C. Garrett, D. G. Truhlar, Criterion of minimum state density in the transition state theory of bimolecular reactions. *J. Chem. Phys.* **70**, 1593–1598 (1979).
11. S. N. Rai, D. G. Truhlar, Variational transition state theory calculations for an atom–radical reaction with no saddle point: O+OH. *J. Chem. Phys.* **79**, 6046–6059 (1983).
12. D. G. Truhlar, B. C. Garrett, Variational transition-state theory. *Acc. Chem. Res.* **13**, 440–448 (1980).
13. A. Fernandez-Ramos, B. A. Ellingson, B. C. Garrett, D. G. Truhlar, Variational transition state theory with multidimensional tunneling. *Rev. Comput. Chem.* **23**, 125–232 (2007).
14. J. L. Bao, D. G. Truhlar, Variational transition state theory: Theoretical framework and recent developments. *Chem. Soc. Rev.* **46**, 7548–7596 (2017).
15. D. M. Wardlaw, R. A. Marcus, Unimolecular reaction rate theory for transition states of partial looseness. II. Implementation and analysis with applications to NO_2 and C_2H_6 dissociations. *J. Chem. Phys.* **83**, 3462–3480 (1985).
16. S. J. Klippenstein, A bond length reaction coordinate for unimolecular reactions. II. Microcanonical and canonical implementations with application to the dissociation of NCNO. *J. Chem. Phys.* **94**, 6469–6482 (1991).
17. S. C. Smith, Microscopic rate coefficients in reactions with flexible transition states: Analysis of the transitional-mode sum of states. *J. Chem. Phys.* **95**, 3404–3430 (1991).
18. Y. Georgievskii, S. J. Klippenstein, Variable reaction coordinate transition state theory: Analytic results and application to the C_2H_3+H→C_2H_4 reaction. *J. Chem. Phys.* **118**, 5442–5455 (2003).
19. Y. Georgievskii, S. J. Klippenstein, Transition state theory for multichannel addition reactions: Multifaceted dividing surfaces. *J. Phys. Chem. A* **107**, 9776–9781 (2003).
20. Y. Georgievskii, S. J. Klippenstein, Long-range transition state theory. *J. Chem. Phys.* **122**, 194103 (2005).
21. J. O. Hirschfelder, E. Wigner, Some quantum-mechanical considerations in the theory of reactions involving an activation energy. *J. Chem. Phys.* **7**, 616–628 (1939).
22. W. H. Miller, Unified statistical model for "complex" and "direct" reaction mechanisms. *J. Chem. Phys.* **65**, 2216–2223 (1976).
23. W. J. Chesnavich, L. Bass, T. Su, M. T. Bowers, Multiple transition states in unimolecular reactions: A transition state switching model. Application to the $C_4H_8^{+\cdot}$ system. *J. Chem. Phys.* **74**, 2228–2246 (1981).
24. S. J. Klippenstein, L. R. Khundkar, A. H. Zewail, R. A. Marcus, Application of unimolecular reaction rate theory for highly flexible transition states to the dissociation of NCNO into NC and NO. *J. Chem. Phys.* **89**, 4761–4770 (1988).
25. W.-P. Hu, D. G. Truhlar, Deuterium kinetic isotope effects and their temperature dependence in the gas-Phase S_N2 reactions $X^- + CH_3Y \rightarrow CH_3X + Y^-$ (X, Y = Cl, Br, I). *J. Am. Chem. Soc.* **117**, 10726–10734 (1995).
26. W.-P. Hu, D. G. Truhlar, Factors affecting competitive ion–molecule reactions: ClO^- + C_2H_5Cl and C_2D_5Cl via E2 and S_N2 channels. *J. Am. Chem. Soc.* **118**, 860–869 (1996).
27. B. C. Garrett, D. G. Truhlar, Canonical unified statistical model. Classical mechanical theory and applications to collinear reactions. *J. Chem. Phys.* **76**, 1853–1858 (1982).
28. F. S. C. Lee, F. S. Rowland, The reaction of chlorine atoms with acetylene and its possible stratospheric significance. *J. Phys. Chem.* **81**, 684–685 (1977).
29. R. Atkinson, S. M. Aschmann, Kinetics of the gas phase reaction of Cl atoms with a series of organics at 296±2 K and atmospheric pressure. *Int. J. Chem. Kinet.* **17**, 33–41 (1985).
30. J. Brunning, L. J. Stief, Pressure dependence of the absolute rate constant for the reaction Cl+C_2H_2 from 210–361 K. *J. Chem. Phys.* **83**, 1005–1009 (1985).
31. T. J. Wallington, L. M. Skewes, W. O. Siegl, Kinetics of the gas phase reaction of chlorine atoms with a series of alkenes, alkynes and aromatic species at 295 K. *J. Photochem. Photobiol. Chem.* **45**, 167–175 (1988).
32. T. J. Wallington, J. M. Andino, I. M. Lorkovic, E. W. Kaiser, G. Marston, Pressure dependence of the reaction of chlorine atoms with ethene and acetylene in air at 295 K. *J. Phys. Chem.* **94**, 3644–3648 (1990).
33. E. W. Kaiser, Pressure dependence of the reaction Cl + C_2H_2 over the temperature range 230 to 370 K. *Int. J. Chem. Kinet.* **24**, 179–189 (1992).
34. E. W. Kaiser, T. J. Wallington, Kinetics of the reactions of chlorine atoms with C_2H_4 (k_1) and C_2H_2 (k_2): A determination of $\Delta H_{f,298}^{\circ}$ for C_2H_3. *J. Phys. Chem.* **100**, 4111–4119 (1996).
35. E. Iwasaki, H. Chiba, T. Nakayama, Y. Matsumi, T. J. Wallington, PLP–LIF study of the reactions of chlorine atoms with C_2H_2, C_2H_4, and C_3H_6 in 2–100Torr of N_2 diluent at 295K. *Chem. Phys. Lett.* **494**, 174–178 (2010).
36. Y. Gao *et al*., Kinetics and thermochemistry of the addition of atomic chlorine to acetylene. *Proc. Combust. Inst.* **31**, 193–200 (2007).
37. L. Zhu, W. Chen, W. L. Hase, E. W. Kaiser, Comparison of models for treating angular momentum in RRKM calculations with vibrator transition states: Pressure and temperature dependence of chlorine atom + acetylene association. *J. Phys. Chem.* **97**, 311–322 (1993).
38. V. D. Knyazev, I. J. Kalinovski, I. R. Slagle, Kinetics of the $CH_2CH_2Cl \rightleftarrows C_2H_4$ + Cl reaction. *J. Phys. Chem. A* **103**, 3216–3221 (1999).
39. E. E. Greenwald, S. W. North, Y. Georgievskii, S. J. Klippenstein, A two transition state model for radical-molecule reactions: A case study of the addition of OH to C_2H_4. *J. Phys. Chem. A* **109**, 6031–6044 (2005).
40. Y. Georgievskii, S. J. Klippenstein, Strange kinetics of the C_2H_6 + CN reaction explained. *J. Phys. Chem. A* **111**, 3802–3811 (2007).
41. H. Sabbah *et al*., Understanding reactivity at very low temperatures: The reactions of oxygen atoms with alkenes. *Science* **317**, 102–105 (2007).
42. J. Li, C. Geng, X. Huang, J. Zhan, C. Sun, F/Cl+C_2H_2 reactions: Are the addition and hydrogen abstraction direct processes? *Chem. Phys.* **331**, 42–54 (2006).
43. D. Polino, S. J. Klippenstein, L. B. Harding, Y. Georgievskii, Predictive theory for the addition and insertion kinetics of ^{1}CH2 reacting with unsaturated hydrocarbons. *J. Phys. Chem. A* **117**, 12677–12692 (2013).
44. M. Monge-Palacios, E. Grajales-González, S. M. Sarathy, Ab initio, transition state theory, and kinetic modeling study of the HO_2-Assisted keto–enol tautomerism propen-2-ol + HO_2 ⇔ acetone + HO_2 under combustion, atmospheric, and interstellar conditions. *J. Phys. Chem. A* **122**, 9792–9805 (2018).
45. K. K. Baldridge, M. S. Gordon, R. Steckler, D. G. Truhlar, Ab initio reaction paths and direct dynamics calculations. *J. Phys. Chem.* **93**, 5107–5119 (1989).
46. Y.-P. Liu, D.-h. Lu, A. Gonzàlez-Lafont, D. G. Truhlar, B. C. Garrett, Direct dynamics calculation of the kinetic isotope effect for an organic hydrogen-transfer reaction, including corner-cutting tunneling in 21 dimensions. *J. Am. Chem. Soc.* **115**, 7806–7817 (1993).
47. Y. Zhao, D. G. Truhlar, The M06 suite of density functionals for main group thermochemistry, thermochemical kinetics, noncovalent interactions, excited states, and transition elements: Two new functionals and systematic testing of four M06-class functionals and 12 other functionals. *Theor. Chem. Acc.* **120**, 215–241 (2008).
48. Y. Zhao, D. G. Truhlar, Exploring the limit of accuracy of the global hybrid meta density functional for main-group thermochemistry, kinetics, and noncovalent interactions. *J. Chem. Theory Comput.* **4**, 1849–1868 (2008).
49. E. Papajak, D. G. Truhlar, Efficient diffuse basis sets for density functional theory. *J. Chem. Theory Comput.* **6**, 597–601 (2010).
50. E. Papajak, D. G. Truhlar, Convergent partially augmented basis sets for Post-Hartree-Fock calculations of molecular properties and reaction barrier heights. *J. Chem. Theory Comput.* **7**, 10–18 (2011).
51. B. J. Lynch, Y. Zhao, D. G. Truhlar, Effectiveness of diffuse basis functions for calculating relative energies by density functional theory. *J. Phys. Chem. A* **107**, 1384–1388 (2003).
52. B. Chan, L. Radom, W2X and W3X-L: Cost-effective approximations to W2 and W4 with kJ $mol^{(-1)}$ accuracy. *J. Chem. Theory Comput.* **11**, 2109–2119 (2015).
53. Y. Zhao *et al*., Extrapolation of high-order correlation energies: The WMS model. *Phys. Chem. Chem. Phys.* **20**, 27375–27384 (2018).

Downloaded by guest on October 22, 2020

54. A. Kuppermann, D. G. Truhlar, Exact tunneling calculations. *J. Am. Chem. Soc.* **93**, 1840–1851 (1971).
55. C. F. Jackels, Z. Gu, D. G. Truhlar, Reaction-path potential and vibrational frequencies in terms of curvilinear internal coordinates. *J. Chem. Phys.* **102**, 3188–3201 (1995).
56. J. Zheng, S. Zhang, D. G. Truhlar, Density functional study of methyl radical association kinetics. *J. Phys. Chem. A* **112**, 11509–11513 (2008).
57. J. Zheng *et al*., Polyrate-Version 2017-C (University of Minnesota, Minneapolis, MN, 2017).
58. J. L. Bao, X. Zhang, D. G. Truhlar, Barrierless association of CF_2 and dissociation of C_2F_4 by variational transition-state theory and system-specific quantum Rice-Ramsperger-Kassel theory. *Proc. Natl. Acad. Sci. U.S.A.* **113**, 13606–13611 (2016).
59. J. Zheng, D. G. Truhlar, Multi-path variational transition state theory for chemical reaction rates of complex polyatomic species: Ethanol + OH reactions. *Faraday Discuss.* **157**, 59–88, discussion 113–140 (2012).
60. B. D. Smith, Simplified calculation of chemical equilibria in hydrocarbon systems containing isomers. *AIChE J.* **5**, 26–28 (1959).
61. R. A. Alberty, Calculation of chemical thermodynamic properties of isomer groups containing fixed-ratio subgroups. *Ind. Eng. Chem. Fundam.* **23**, 129–130 (1984).
62. X. Xu, I. M. Alecu, D. G. Truhlar, How well can modern density functionals predict internuclear distances at transition states? *J. Chem. Theory Comput.* **7**, 1667–1676 (2011).
63. S. P. Sander *et al*., *Chemical Kinetics and Photochemical Data for Use in Atmospheric Studies: Evaluation Number 14* (NASA Jet Propulsion Laboratory, Pasadena, CA, 2003).
64. J. B. Burkholder *et al*., *Chemical Kinetics and Photochemical Data for Use in Atmospheric Studies: Evaluation Number 18* (NASA Jet Propulsion Laboratory, Pasadena, CA, 2015).
65. J. Zheng, R. Meana-Pañeda, D. G. Truhlar, Prediction of experimentally unavailable product branching ratios for biofuel combustion: The role of anharmonicity in the reaction of isobutanol with OH. *J. Am. Chem. Soc.* **136**, 5150–5160 (2014).
66. A. D. Isaacson, D. G. Truhlar, Polyatomic canonical variational theory for chemical reaction rates. Separable-mode formalism with application to $OH+H_2 \rightarrow H_2O+H$. *J. Chem. Phys.* **76**, 1380–1391 (1982).
67. Z. Chen, Rotation procedure in intrinsic reaction coordinate calculations. *Theor. Chim. Acta* **75**, 481–484 (1989).

Downloaded by guest on October 22, 2020